Selective autophagy of AKAP11 activates cAMP/PKA to fuel mitochondrial metabolism and tumor cell growth

Zhiqiang Deng[a,b], Xianting Li[a,b], Marian Blanca Ramirez[a,b], Kerry Purtell[a,b], Insup Choi[a,b], Jia-Hong Lu[c], Qin Yu[d], and Zhenyu Yue[a,b,1]

[a]Department of Neurology, The Friedman Brain Institute, Icahn School of Medicine at Mount Sinai, New York, NY 10029; [b]Department of Neuroscience, The Friedman Brain Institute, Icahn School of Medicine at Mount Sinai, New York, NY 10029; [c]State Key Laboratory of Quality Research in Chinese Medicine, Institute of Chinese Medical Sciences, University of Macau, 999078 Macau SAR, China; and [d]Department of Oncological Sciences, Icahn School of Medicine at Mount Sinai, New York, NY 10029

Autophagy is a catabolic pathway that provides self-nourishment and maintenance of cellular homeostasis. Autophagy is a fundamental cell protection pathway through metabolic recycling of various intracellular cargos and supplying the breakdown products. Here, we report an autophagy function in governing cell protection during cellular response to energy crisis through cell metabolic rewiring. We observe a role of selective type of autophagy in direct activation of cyclic AMP protein kinase A (PKA) and rejuvenation of mitochondrial function. Mechanistically, autophagy selectively degrades the inhibitory subunit RI of PKA holoenzyme through A-kinase–anchoring protein (AKAP) 11. AKAP11 acts as an autophagy receptor that recruits RI to autophagosomes via LC3. Glucose starvation induces AKAP11-dependent degradation of RI, resulting in PKA activation that potentiates PKA-cAMP response element-binding signaling, mitochondria respiration, and ATP production in accordance with mitochondrial elongation. AKAP11 deficiency inhibits PKA activation and impairs cell survival upon glucose starvation. Our results thus expand the view of autophagy cytoprotection mechanism by demonstrating selective autophagy in RI degradation and PKA activation that fuels the mitochondrial metabolism and confers cell resistance to glucose deprivation implicated in tumor growth.

AKAP11 | PKA | autophagy | mitochondrial metabolism | cell survival

Macroautophagy (henceforth autophagy) is a catabolic process that degrades various cellular cargos through lysosomes. The autophagy process includes the formation and trafficking of autophagosomes, which sequester the cellular cargos destined for the clearance. Autophagy is activated in response to nutrient deprivation or cellular injuries and serves as a recycling mechanism that maintains cellular homeostasis through degradation of cytoplasmic components. Autophagy provides cell self-nourishment and supports cellular metabolism by supplying breakdown products (1, 2); therefore, autophagy is a fundamental cell protection mechanism. Whether autophagy has a direct function beyond recycling of the breakdown molecules to maintain metabolic homeostasis and cell survival, however, is poorly understood. In certain cancer types, autophagy plays an important role in sustaining the aggressive growth of the tumor cells by enhancing cell metabolism. Although our group and others have previously shown an inhibitory function of Beclin 1–mediated autophagy in tumorigenesis (3, 4), the current view is that tumors, once established, rely heavily on autophagy to survive due to high metabolic demand. One potential mechanism is that the metabolic products generated by autophagy provide tumor cells with metabolic rewiring that enables them to survive even under nutrient-poor conditions (5, 6). However, it remains unclear whether autophagy plays a role beyond the production of metabolic fuel sources to maintain metabolic plasticity and tumor cell growth.

Available evidence has demonstrated the selectivity of autophagy in the digestion of certain cellular cargoes mediated by autophagy adaptors/receptors. Characterization of the autophagy adaptors has shed light on the versatile physiological function of autophagy in the maintenance of the homeostasis for large molecules and cellular organelles (7, 8). These adaptors recognize and recruit selective cargos to autophagy machinery for degradation through direct interaction with yeast autophagy gene Atg8 homologs of mammalian LC3/GABARAP/Gate16 proteins. While a few autophagy receptors have been reported, it is clear that many more are yet to be identified (7, 8).

The best-known signaling pathways that control the metabolic stress-induced autophagy are mediated by mTOR and AMPK kinases, both of which are the master regulators for cellular metabolism (9, 10). Cyclic adenosine monophosphate (cAMP)-dependent protein kinase (PKA) is also a key kinase of cell metabolism that governs diverse cellular pathways, including cellular glucose metabolism and bioenergetic processes (11–13). Surprisingly, whether and how cAMP/PKA regulates autophagy or vice versa is poorly understood in mammals (14–16). cAMP/PKA signaling has emerged over recent years as a key regulator for mitochondrial functions, highlighting the mechanism of cAMP/PKA in cellular metabolism control (17, 18). Despite an established role for PKA in the regulation of mitochondrial metabolism, whether autophagy and PKA converge to regulate metabolic reprogramming and cell survival remains unknown.

The PKA holoenzyme consists of two regulatory subunits (R) and two catalytic subunits (C). The R subunits are inhibitory of catalytic kinase activity; upon binding to cAMP, the R subunit dissociates from C subunit, resulting in activation of PKA (19).

Significance

Autophagy is known to promote cell survival through providing various sources of fuels as a result of digestion. Here, we uncover a function of autophagy in cell metabolic regulation by directly activating cAMP/PKA signaling that fuels mitochondrial metabolism and confers cell resistance to energy crisis. We find that autophagy selectively degrades PKA inhibitory subunit RIα through new autophagy receptor AKAP11 in response to energy crisis, thus causing PKA activation, which is a central hub for a variety of cellular signaling. Our study suggests that tumor cells may exploit such a metabolic reprogramming mechanism for the oncogenic growth. We propose that AKAP11-mediated cAMP/PKA activation via selective autophagy should be explored in the future as a therapeutic target for cancer treatment.

CELL BIOLOGY

Furthermore, the specific cellular functions of PKA are controlled by a number of A-kinase–anchoring proteins (AKAPs). The AKAPs bind the R subunits and restrict the PKA holoenzyme to various intracellular compartments, providing spatiotemporal regulation of PKA activity (20). However, the functions of many AKAPs are poorly characterized.

Here, we report a role of autophagy that controls cellular metabolism beyond the production of metabolic sources—it activates cAMP/PKA kinase activity by selective degradation of the inhibitory subunit of R1α through autophagy receptor AKAP11 in response to glucose starvation. AKAP11-mediated cAMP/PKA activation leads to elevation of mitochondrial metabolism and cell protection. Our study reveals a previously unrecognized function of autophagy in metabolic rewiring of cells that promote cell survival under energy crisis. Our study thus suggests that selective autophagy induced RI degradation and PKA activation may contribute to the resistance of tumor cells to metabolic stress.

Results

Autophagy Is Required for PKA Activation and Cell Viability upon Glucose Starvation. The functional relationship between PKA and autophagy is largely unclear. Because PKA controls cell metabolism particularly related to glucose status (21–23), we first examined the relationship between autophagy and PKA activity in the control of cell metabolism with glucose limitation. We found that in addition to activating autophagy, glucose starvation also induced the phosphorylation of cAMP response element-binding (p-CREB), a well-known PKA substrate, indicative of elevated PKA activity in both HEK293T and HCT116 cells. In contrast, disruption of autophagy by deletion of essential autophagy gene *Atg7* or *Atg14* abolished the increase of p-CREB levels in the above cells (*SI Appendix*, Fig. S1 *A, B, D, and E*), suggesting that inactivation of autophagy suppresses PKA activity in response to energy shortage. Moreover, loss of *Atg7* or *Atg14* accelerated cell death in response to glucose starvation (*SI Appendix*, Fig. S1 *C and F*). Taken together, our results show that autophagy is required for PKA activation and important for cell viability under metabolic stress.

Autophagy Degrades PKA-Associated Proteins AKAP11 and RIα. To dissect the mechanism whereby autophagy controls PKA activity, we searched for proteins associated with PKA that are potentially regulated by autophagy. The type I PKA regulatory subunit α (RIα) and anchoring protein AKAP11, which are encoded by *PRKAR1A* and *AKAP11* genes, respectively, were shown to associate with autophagy protein LC3 (7). We observed that both protein levels were significantly increased in autophagy-deficient mouse tissues (*Atg7^{F/F}-SynCre* and *Atg14^{F/F}-SynCre* mice), mouse embryonic fibroblasts (MEFs) (*Atg7^{−/−}*) and human HEK293T cells (*Atg7^{−/−}*), while the messenger RNA (mRNA) levels of *AKAP11* and *PRKAR1A* are unaltered in autophagy-deficient cells (Fig. 1 *A–D* and *SI Appendix*, Fig. S2 *A–E*). To test their degradation by autophagy, we induced autophagy in MEFs and HEK293T cells by nutrient starvation and found reduction of RIα and AKAP11 proteins in wild type (WT) but not in autophagy-deficient (*Atg7^{−/−}*) cells (Fig. 1 *E–H*), consistent with an autophagy-dependent degradation. Furthermore, the degradation of RIα and AKAP11 caused by nutrient limitation was prevented in cells treated with bafilomycin A1 (*SI Appendix*, Fig. S2 *F–I*). In contrast, the level of RIIα was not altered when autophagy was either blocked or induced (Fig. 1 and *SI Appendix*, Fig. S2). The results suggest that autophagy specifically degrades AKAP11 and RIα.

AKAP11 Is an Autophagy Receptor That Interacts with LC3. AKAP11 is an anchor protein belonging to the AKAP family that targets PKA to discrete subcellular compartments through RIα binding (24, 25). We hypothesize that AKAP11 is an autophagy receptor that targets RIα to autophagy degradation. To test this idea, we first investigated if AKAP11 interacts with LC3, an autophagy

protein localized at the autophagosome after posttranslational processing (26). Glutathione S-transferase (GST)-tagged LC3A, LC3B, or GABARAP fusion proteins were purified and incubated with HEK293T cell lysates expressing HA-tagged AKAP11 protein, followed by pull-down with GST beads. GST-LC3A, GST-LC3B, or GST-GABARAP, but not GST alone, pulled down HA-AKAP11 (Fig. 2*A* and *SI Appendix*, Fig. S3*A*). In HEK293T cells stably expressing green fluorescent protein (GFP)-LC3B, endogenous AKAP11 was coimmunoprecipitated (co-IP) with GFP-LC3B (Fig. 2*B*). We found that AKAP11 contains a conserved LC3-interacting region (LIR) WSNL at the C-terminal domain (27) (Fig. 2*C*). Substitution of the WSNL with four alanine residues (WSNL/AAAA, mutLIR) significantly impaired the interaction of mutant AKAP11 with LC3B in the above GST pull-down and GFP-LC3B (or HA-AKAP11) co-IP assays (Fig. 2 *D–F* and *SI Appendix*, Fig. S3*B*). We noticed that the mutLIR AKAP11 did not completely lose the interaction with LC3B; the residual binding could implicate other site of AKAP11 in LC3B interaction. Expression of HA-AKAP11 WT, but not mutLIR, results in discrete puncta containing both endogenous autophagosomal protein LC3 and HA-AKAP11 upon nutrient starvation plus Baf A1 treatment (Fig. 2 *G–I*). These results suggest that recruitment of AKAP11 to autophagosomes depends on the interaction between LIR in AKAP11 and LC3.

AKAP11 Mediates RIα Recruitment to Autophagosomes for Degradation. We next generated *AKAP11* knockout (KO) HEK293T and HeLa cells through CRISPR-Cas9 editing to investigate the function of endogenous AKAP11. The protein level of RIα, but not RIIα, was significantly increased in both HEK293T and HeLa *AKAP11* KO cell lines, while the mRNA level of *PRKAR1A* was not increased in *AKAP11* KO cells (Fig. 3 *A–D* and *SI Appendix*, Fig. S3*C*), confirming the role for AKAP11 in RIα degradation. The results were verified in independent clones of *AKAP11* KO cells generated through different guide RNA (*SI Appendix*, Fig. S3*D*). Furthermore, induction of autophagy via starvation triggers the reduction of RIα levels in WT cells but not in *AKAP11* KO HEK293T (Fig. 3 *E* and *F*) and HeLa cells (Fig. 3 *G* and *H*). Expression of FLAG-RIα also leads to the formation of punctate structures, which colocalize with endogenous LC3-associated autophagosomes upon nutrient starvation plus Baf A1 treatment (Fig. 3 *I–K*). In contrast, RIα puncta formation was abolished in *AKAP11* KO cells under the same conditions (Fig. 3 *I–K*), demonstrating the requirement of AKAP11 for the recruitment of RIα to autophagosomes. Moreover, FLAG-LC3 was co-IPed with endogenous RIα (or AKAP11) using anti-FLAG antibody in WT but completely lost in *AKAP11* KO cells (Fig. 3*L*). Similar results were found in *AKAP11* knockdown cells stably expressing GFP-LC3B (*SI Appendix*, Fig. S3 *E and F*). Reintroducing AKAP11 by expression of HA-AKAP11 in *AKAP11* KO cells recovered RIα levels when co-IPed with FLAG-LC3, whereas HA-AKAP11 mutLIR expression exhibited poor efficiency in co-IP with FLAG-LC3 and RIα (Fig. 3 *L and M*). We performed co-IP experiments with stably expressing GFP-LC3B HEK293T cells, which were further transfected with either FLAG-RIα/HA-AKAP11 or FLAG-RIα/HA-AKAP11 mutLIR. The result showed that the LIR motif of AKAP11 is necessary for the interaction between LC3B and RIα proteins (*SI Appendix*, Fig. S3 *G–J*). Taken together, our results demonstrate that AKAP11 mediates the autophagic degradation of RIα through the conserved LIR in AKAP11 for LC3 interaction.

Glucose Deprivation Causes AKAP11-Dependent PKA Activation. Given RIα inhibitory function in PKA activity, we next asked whether AKAP11-mediated autophagic degradation of RIα affects PKA activity by assaying p-CREB, a well-known substrate of PKA (28). We found no difference in the levels of p-CREB, total CREB, or their ratio, between WT and *AKAP11* KO cells under basal conditions (*SI Appendix*, Fig. S4 *A and B*) or nutrient starvation with
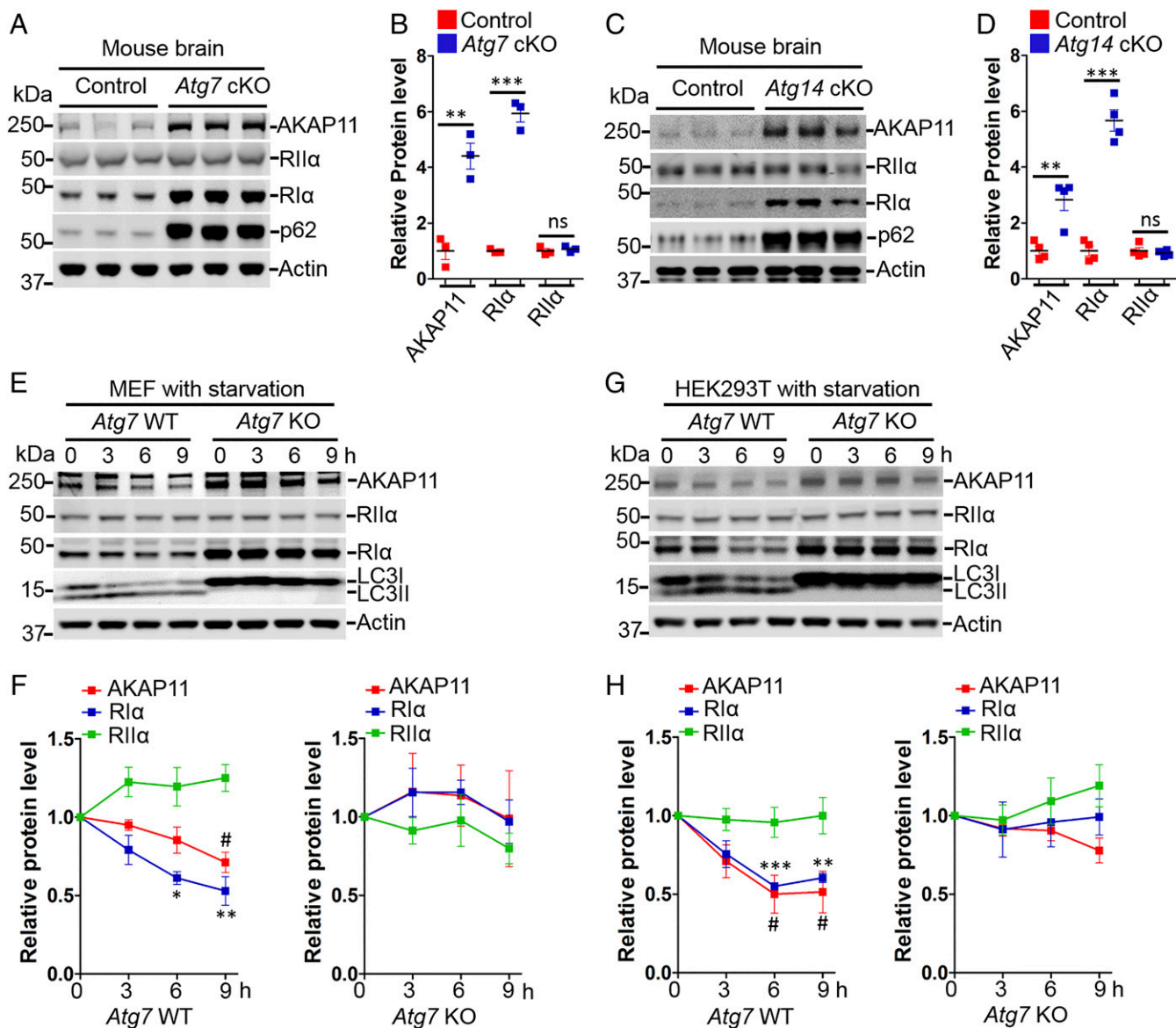
Fig. 1. AKAP11 and RIα are degraded by autophagy. (*A*) Brain lysates of *Atg7^F/F* (Control) and *Atg7^F/F-SynCre* (cKO) were subjected to immunoblotting analysis with the indicated antibodies. (*B*) Quantification of protein levels in *A*. Unpaired Student's *t* tests were used, and values are presented as mean ± SEM (*n* = 3 mice/genotype). **$P < 0.01$; ***$P < 0.001$; ns, not significant. (*C*) Brain lysates of *Atg14^F/F* (Control) and *Atg14^F/F-SynCre* (cKO) were subjected to immunoblotting analysis with the indicated antibodies. (*D*) Quantification of protein levels in *C*. Unpaired Student's *t* tests were used, and values are presented as mean ± SEM (*n* = 4 mice/genotype). **$P < 0.01$; ***$P < 0.001$; ns, not significant. (*E*) *Atg7* WT and *Atg7* KO MEF cells were nutrient starved by using EBSS for the indicated times, and cells were assayed by immunoblotting analysis with the indicated antibodies. (*F*) Quantification of the protein levels from *E* was obtained by normalizing the level of proteins to Actin, respectively, and further to the respective control. One-way ANOVA was used in each genotype, and values are presented as mean ± SEM (*n* = 3). *$P < 0.05$; **$P < 0.01$. (*G*) *Atg7* WT and *Atg7* KO HEK293T cells were nutrient starved by using EBSS for the indicated times and were then assayed by immunoblotting analysis with the indicated antibodies. (*H*) Quantification of the protein levels from *G* was obtained by normalizing the level of proteins to Actin, respectively, and further to the respective control. One-way ANOVA was used in each genotype, and values are presented as mean ± SEM (*n* = 4). #$P < 0.05$; **$P < 0.01$; ***$P < 0.001$.

Earle's balanced salts solution (EBSS) treatment (*SI Appendix,* Fig. S4 *C* and *D*); despite that, AKAP11 and RIα levels are reduced under EBSS treatment (Fig. 3 *E* and *F*). We then investigated the impact of AKAP11 on PKA activity with glucose limitation. We utilized a fluorescence resonance energy transfer (FRET)-based biosensor to monitor PKA activity in live cells upon glucose starvation (29). While PKA activity was elevated upon glucose starvation as previously reported in WT cells (30, 31), it changed little in *AKAP11* KO cells (Fig. 4 *A* and *B*). This observation was corroborated by the evidence of elevated p-CREB levels in WT but unchanged in *AKAP11* KO cells (both HEK293T and

HeLa cells) upon glucose starvation (Fig. 4 *C* and *D* and *SI Appendix,* Fig. S5 *A* and *B*). As glucose starvation also induces autophagy, we observed that AKAP11 and RIα total protein levels declined over the course of glucose starvation in WT cells, whereas the reduction in RIα levels was prevented in *AKAP11* KO cells (Fig. 4 *C* and *E* and *SI Appendix,* Fig. S5 *A* and *C*). Remarkably, overexpression of *AKAP11*-mutLIR, but not *AKAP11*-WT, in WT HEK293T causes accumulation of endogenous RIα protein and further prevents RIα degradation induced by glucose starvation (*SI Appendix,* Fig. S6 *A* and *B*), suggesting a dominant negative effect of mutLIR variant on RIα degradation. In *AKAP11* KO cells,
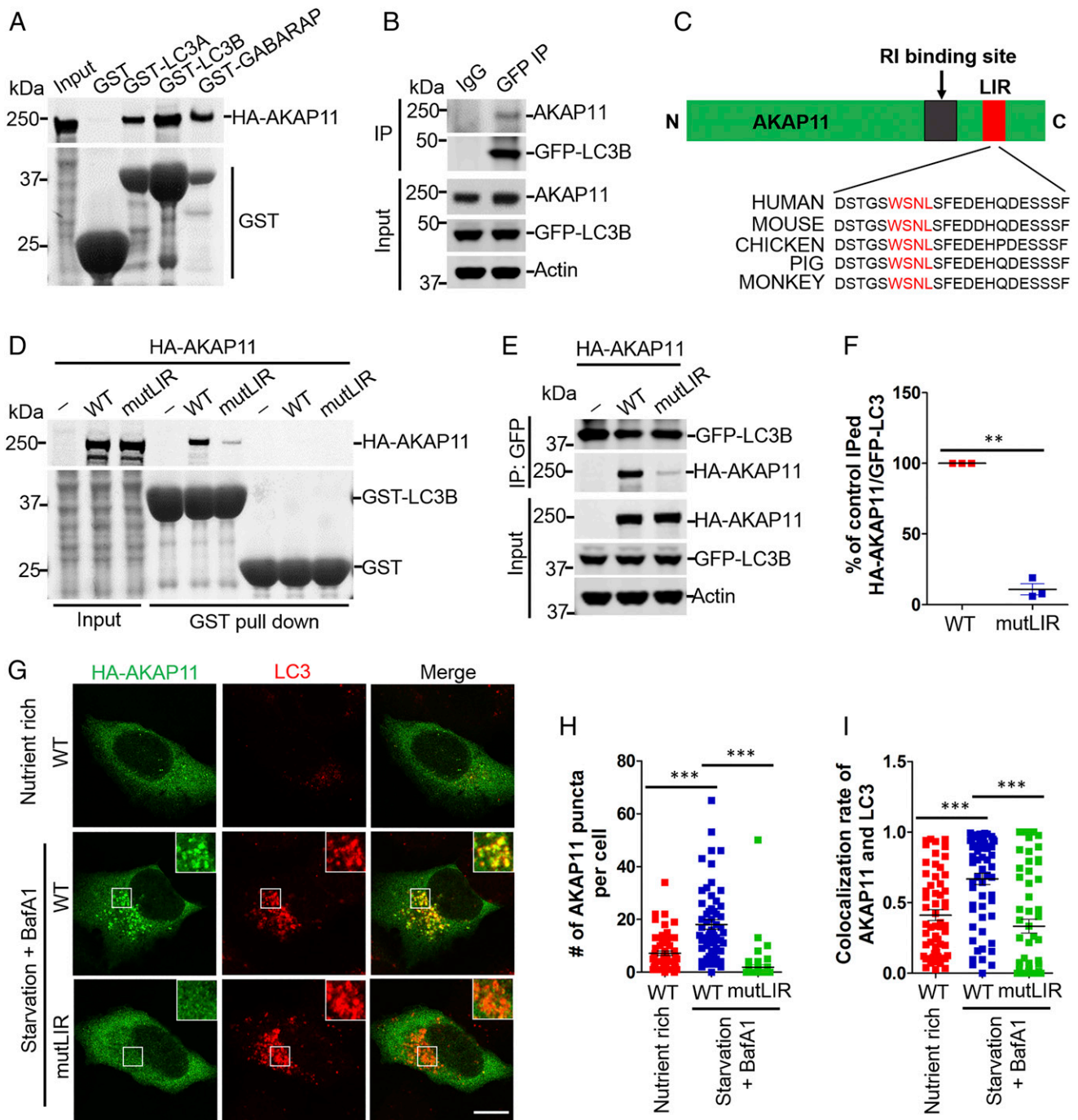
CELL BIOLOGY

Fig. 2. AKAP11 is an autophagy adaptor harboring LC3-interacting region. (*A*) Purified GST, GST-LC3A, GST-LC3B, or GST-GABARAP proteins were incubated with HEK293T lysates expressing HA-AKAP11 and subjected to pull-down assay. Interaction of HA-AKAP11 and GST-fusion proteins was detected by immunoblotting analysis with the indicated antibodies. (*B*) HEK293T cells stably expressing GFP-LC3B were subjected to GFP immunoprecipitation. Interaction of AKAP11 and GFP-LC3B was detected by immunoblotting analysis with the indicated antibodies. (*C*) The alignment of LIR (LC3-interacting region) motif in AKAP11 from different species. (*D*) GST and GST-LC3B were subjected to pull down in HEK293T cellular lysates in the presence of HA-AKAP11-WT and mutLIR. Interaction of HA-AKAP11 and GST-LC3B was detected by immunoblotting analysis with the indicated antibodies. (*E*) HEK293T cells stably expressing GFP-LC3B were transfected with HA-AKAP11-WT or HA-AKAP11-mutLIR. Cellular lysates were subjected to GFP immunoprecipitation. Interaction of HA-AKAP11 and GFP-LC3B was detected by immunoblotting analysis with the indicated antibodies. (*F*) Quantification of the results from *E* was obtained by normalizing levels of immunoprecipitated HA-AKAP11 to the level of input and then further normalizing to the level of immunoprecipitated GFP-LC3B. Paired Student's *t* tests were used, and values are presented as the mean $\pm$ SEM ($n = 3$). **$P < 0.01$. (*G*) HeLa cells transfected with HA-AKAP11 were subjected to nutrient starvation in the presence of Baf A1 and followed by immunostaining with anti-HA and anti-LC3 antibodies. Representative images are shown. (Scale bar, 10 μm.) (*H* and *I*) Quantification of the results from *G*. One-way ANOVA was used, and values are presented as mean $\pm$ SEM (more than 50 cells were calculated from three independent experiments). ***$P < 0.001$.
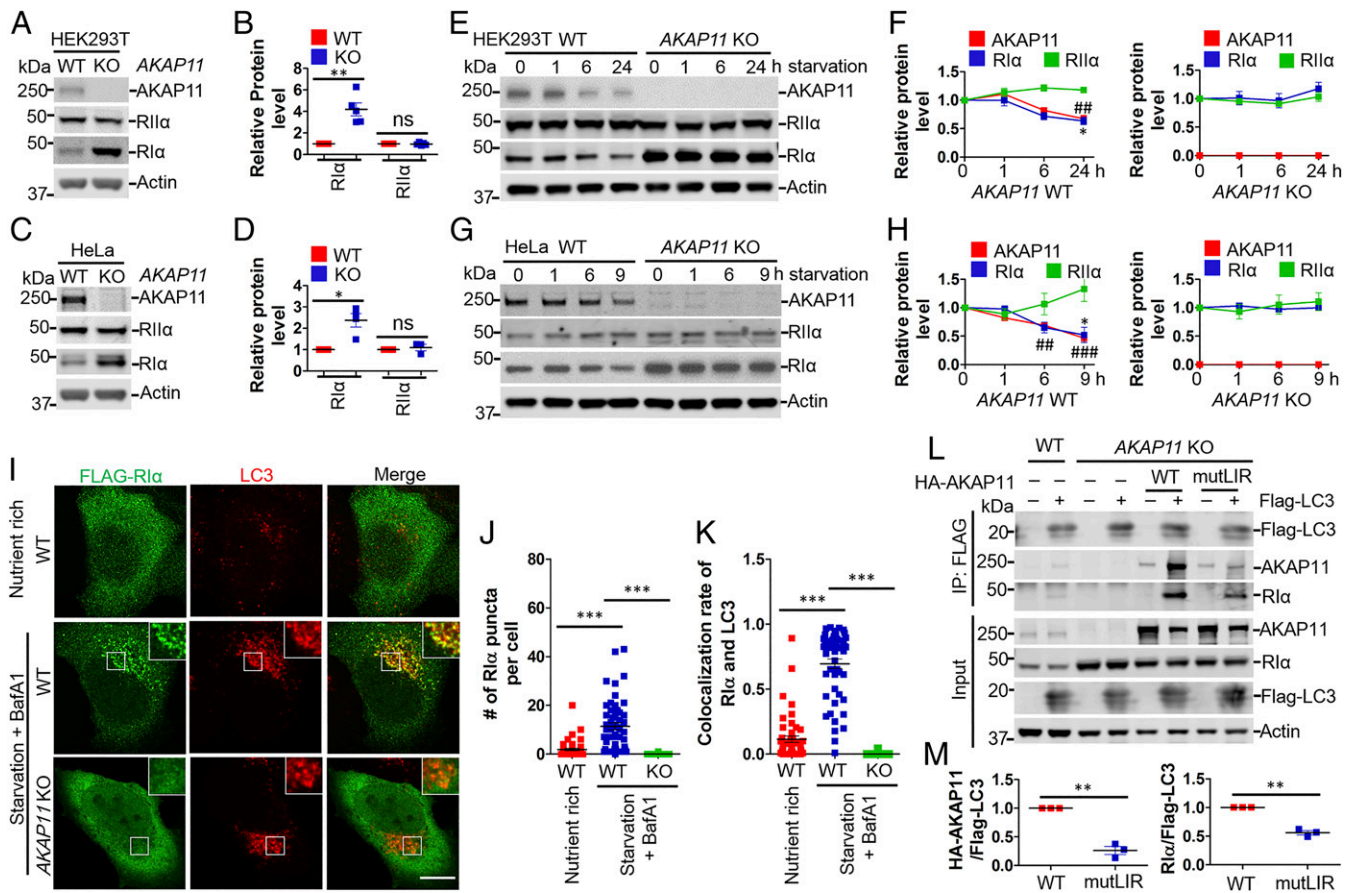
Fig. 3. AKAP11 mediates RIα degradation. WT and *AKAP11* KO HEK293 (*A*) and HeLa (*C*) cells were assayed by immunoblotting analysis with the indicated antibodies. (*B* and *D*) Quantification of the results from *A* and *C* were obtained by normalizing protein levels to Actin, respectively, and further to the respective control. Paired Student's *t* tests were used, and values are presented as the mean ± SEM (*A*, n = 5; *C*, n = 4). *P < 0.05; **P < 0.01; ns, not significant. WT and *AKAP11* KO HEK293 (*E*) and HeLa (*G*) cells were subjected to nutrient starvation by using EBSS, and cells were then assayed by immunoblotting analysis with the indicated antibodies. (*F* and *H*) Quantification of the results from *E* and *G* were obtained by normalizing protein levels to Actin, respectively, and further to the respective control. One-way ANOVA was used in each genotype, and values are presented as mean ± SEM (n = 3). * and #P < 0.05; ##P < 0.01; ###P < 0.001. (*I*) WT and *AKAP11* KO HeLa cells were transfected with FLAG-RIα and subjected to nutrient starvation in the presence of Baf A1. Cells were then immunostained with anti-FLAG and anti-LC3 antibodies. (Scale bar, 10 μm.) (*J* and *K*) Quantification of the results from *I*. One-way ANOVA was used, and values are presented as the mean ± SEM (more than 40 cells were calculated from three independent experiments). ***P < 0.001. (*L*) WT and *AKAP11* KO HEK293T cells were cotransfected with FLAG-LC3 construct, and either HA-AKAP11-WT or HA-AKAP11-mutLIR and were assayed by immunoprecipitation with anti-FLAG antibody. The interaction of FLAG-LC3 and HA-AKAP11 as well as FLAG-LC3 and RIα was detected with the indicated antibodies. (*M*) Quantification of the results from *L* was obtained by normalizing levels of immunoprecipitated HA-AKAP11 and RIα to the level of input and further to the level of immunoprecipitated FLAG. Paired Student's *t* tests were used, and values are presented as the mean ± SEM (n = 3). **P < 0.01.

glucose starvation failed to induce RIα degradation, whereas transfection of *HA-AKAP11* WT, but not *HA-AKAP11*-mutLIR construct, rescues the degradation of RIα (*SI Appendix*, Fig. S6 *C* and *D*). Taken together, glucose deprivation not only induces autophagy but importantly also causes PKA activation through the AKAP11-mediated autophagic degradation of RIα.

AKAP11 Regulates PKA-Mediated Mitochondrial Metabolism in Response to Glucose Deprivation. Current evidence demonstrates that energy crisis (e.g., glucose starvation) causes up-regulation of mitochondrial oxidative phosphorylation (OXPHOS) (32, 33). PKA plays an important role in regulating mitochondrial OXPHOS by controlling the expression or phosphorylation of proteins in the respiratory chain (34–37). We thus investigated whether *AKAP11* deficiency affects mitochondrial respiration by examining oxygen consumption rates (OCRs). The results indicated that WT cells showed glucose-sensitive oxygen consumption, while *AKAP11* KO cells displayed a significant decrease in the basal respiration, maximal respiration, and ATP production upon glucose starvation (Fig. 5 *A* and *B* and *SI Appendix*, Fig. S7 *A* and *B*). In addition, reintroduction of AKAP11-

WT, but not AKAP11-mutLIR, into *AKAP11* KO cells restored the basal respiration, maximal respiration, and ATP production to the levels comparable to WT cells (Fig. 5 *C* and *D*). To verify that reduced mitochondrial OXPHOS in *AKAP11* KO cells is due to compromised PKA activity, we treated cells with FSK/IBMX (to stimulate PKA activity) and examined mitochondrial respiration levels. We found the FSK/IBMX treatment was able to rescue the impaired basal respiration and ATP production in *AKAP11* KO cells to the similar levels of WT cells (Fig. 5 *E* and *F*). The similar results were observed by using HeLa *AKAP11* KO cells generated with different guide RNA (*SI Appendix*, Fig. S7 *C* and *D*). Moreover, we investigated the potential mechanism whereby the loss of AKAP11 disrupts mitochondrial respiration through the blockage of PKA activity in *AKAP11* KO cells. Glucose deprivation activates the PKA-CREB signaling pathway (Fig. 4 and *SI Appendix*, Fig. S5), which results in the potentiation of p-CREB–targeted genes related to mitochondrial respiratory chain complex (37). Upon glucose deprivation, both targets of p-CREB, NDUFS4 (complex I), and MTCOII (complex IV) (38) were increased at the levels of both protein and mRNA in WT cells. In contrast, such increases of both
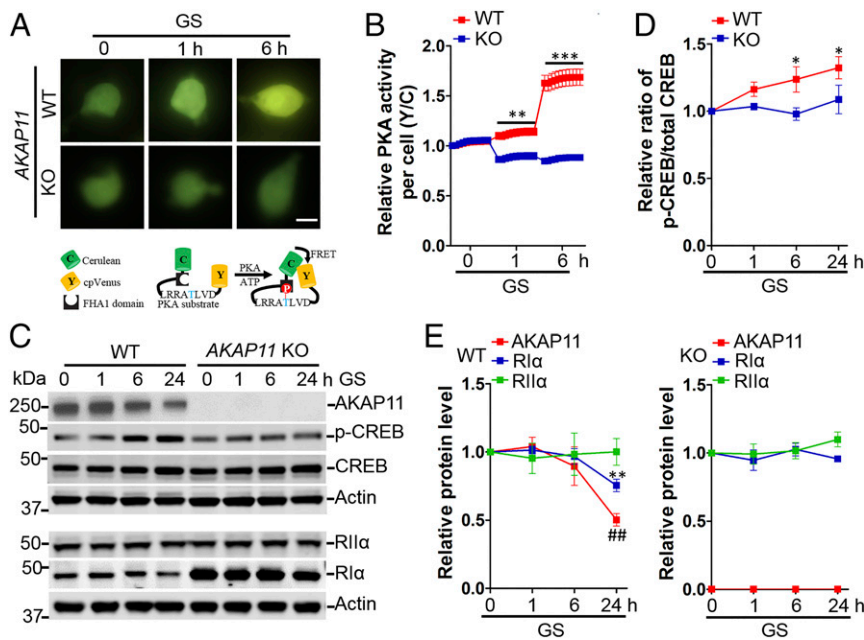
CELL BIOLOGY

Fig. 4. Glucose deprivation causes AKAP11-dependent PKA activation. (*A* and *B*) WT and *AKAP11* KO HEK293T cells were transfected with AKAR4 biosensor construct; at 24 h posttransfection, cells were subjected to glucose starvation (GS) for the indicated time and were then assayed by performing live imaging for 5 min at indicated time points. (*A*, *Top*) Representative images are shown. (Scale bar, 10 μm.) (*Bottom*) Scheme of AKAR4 biosensor. (*B*) Quantification of the results from *A* was obtained by calculating the ratio of Y (the intensity of cpVenus) and C (the intensity of Cerulean) and was then further normalized to each control. Two-way ANOVA was used, and values are presented as mean ± SEM (around 40 cells were calculated from three independent experiments). ***$P < 0.001$. (*C*) WT and *AKAP11* KO HEK293T cells were subjected to GS for the indicated times and were then assayed by immunoblotting analysis with the indicated antibodies. (*D*) Quantification of the results from *C* was obtained by normalizing p-CREB to total CREB levels and further to the respective control. Two-way ANOVA was used, and values are presented as mean ± SEM ($n = 7$). *$P < 0.05$. (*E*) Quantification of the results from *C* was obtained by normalizing the level of proteins to Actin, respectively, and further to the respective control. One-way ANOVA was used for each genotype, and values are presented as mean ± SEM ($n = 7$). ** and ##$P < 0.01$.

mitochondrial proteins and mRNAs were suppressed in *AKAP11* KO cells (Fig. 5 *G* and *H* and *SI Appendix*, Figs. S7 *E* and *F* and S8 *A* and *B*). Thus, we conclude that AKAP11 is required for the activation of mitochondrial metabolism upon glucose starvation through regulating PKA-CREB signaling pathway.

AKAP11 Controls Mitochondrial Elongation and Cell Viability through PKA Phosphorylation of DRP1 upon Glucose Starvation. Growing evidence has demonstrated that glucose deprivation promotes mitochondrial elongation through PKA-induced DRP1 phosphorylation at Ser-637 (p-S637) to maintain mitochondrial metabolism and cell viability (32, 39). We found that mitochondria became elongated upon glucose starvation in WT, but not in *AKAP11* KO cells, by either immunofluorescent analysis (Fig. 6 *A* and *B*) or electron microscopic examination of ultrastructure (Fig. 6*C*). Moreover, we demonstrate an increase in p-S637 DRP1 levels upon glucose starvation in WT cells but no change in *AKAP11* KO cells (Fig. 6 *D* and *E*). Loss of AKAP11 also promoted a remarkable acceleration of cell death following glucose starvation (Fig. 6 *F* and *G* and *SI Appendix*, Figs. S9 *A* and *B* and S10*A*). Furthermore, expression of *AKAP11*-WT, but not mutLIR, was able to prevent cell death in *AKAP11* KO cells upon glucose starvation (Fig. 6*G*). To determine whether the accelerated cell death in *AKAP11* KO cell upon glucose starvation is due to the disruption of RIα degradation, we silenced the expression of *PRKAR1A* in *AKAP11* KO cell by small interfering RNA (siRNA) treatment. The results indicated that compared to scramble siRNA, knockdown of *PRKAR1A* significantly reduced the cell death level in *AKAP11* KO cell upon glucose starvation (Fig. 6*H* and *SI Appendix*, Fig. S10 *B* and *C*). Taken together, our results show that AKAP11 regulates PKA-mediated DRP1 phosphorylation and mitochondria elongation, demonstrating the

role for AKAP11 in controlling metabolic activation (Fig. 5) and cell viability upon glucose starvation.

AKAP11 Is Required for PKA Activation and Growth of Tumor Cells In Vitro. So far, our data has shown that autophagy-dependent PKA activation through AKAP11 is critical to the up-regulation of metabolism and cell protection upon glucose starvation. To ask if such a mechanism contributes to tumor cell resistance to glucose limitation, we next investigated the role for AKAP11 in tumor cell growth. As a proof of principle trial, we first examined AKAP11 protein levels in five established human glioblastoma cell lines; indeed, all five lines showed increased abundance compared to HeLa cells (Fig. 7 *A* and *B*). We then knocked down the expression of *AKAP11* by using short hairpin RNA (shRNA) transduction in U87, U251, and SF763 cells and found a significant increase of RIα but not RIIα protein (Fig. 7 *C* and *D*). Treatment of the glioblastoma cells with 2-Deoxy-D-glucose (2-DG), a glucose analog that blocks glucose metabolism, resulted in increased PKA activity as evidenced by elevated p-CREB levels in control but not in *AKAP11* shRNA knockdown cells (Fig. 7 *E* and *F*). Knockdown of *AKAP11* also significantly sensitized the tumor cells to 2-DG–induced cell death at 24 h posttreatment (Fig. 7*G*). We next performed colony formation assay with the tumor cells and observed a significant reduction of the colony numbers in the tumor cells deficient in *AKAP11* compared to the ones infected with non-targeting shRNA (control) (Fig. 7 *H* and *I*). Therefore, we conclude that reduced expression of *AKAP11* inhibits PKA activation and suppresses oncogenic growth of tumor cells in cultures.

Discussion

Our study uncovers a cytoprotection mechanism whereby autophagy controls cell metabolism beyond production of digested
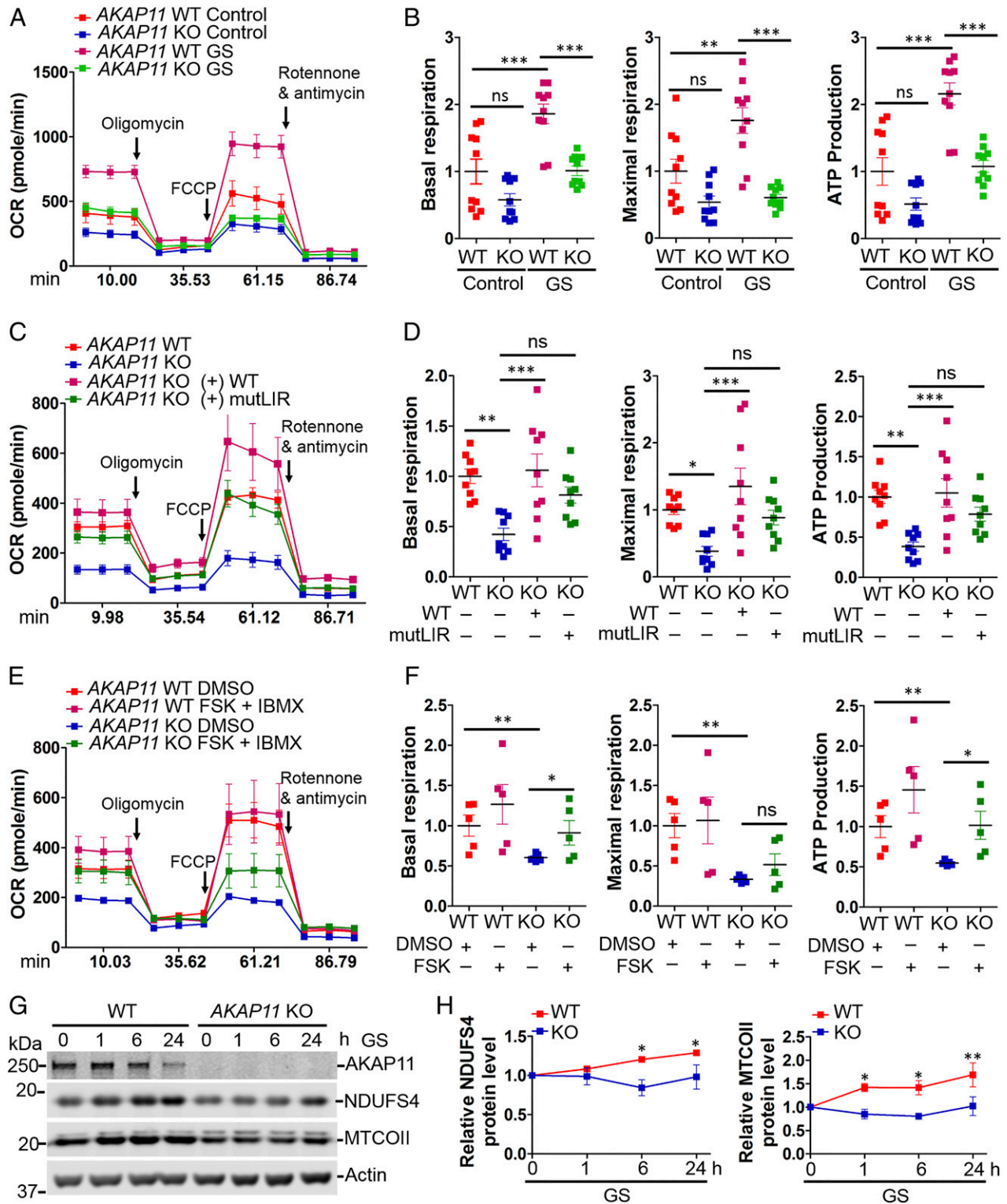
Fig. 5. AKAP11 regulates PKA-mediated mitochondrial metabolism in response to glucose starvation (GS). (*A* and *B*) WT and *AKAP11* KO HEK293T cells were treated with GS for 1 h and were then subjected to seahorse assay. One-way ANOVA was used. Data are presented as mean $\pm$ SEM ($n = 10$ biological replicates). **$P < 0.01$; ***$P < 0.001$; ns, not significant. (*C* and *D*) WT and *AKAP11* KO HEK293T cells were transfected with AKAP11-WT or mutLIR constructs and subjected to seahorse assay with low glucose medium. One-way ANOVA was used. Data are presented as mean $\pm$ SEM ($n = 9$ biological replicates). *$P < 0.05$; **$P < 0.01$; ***$P < 0.001$; ns, not significant. (*E* and *F*) WT and *AKAP11* KO HEK293T cells were treated with either DMSO or 20 μM forskolin (FSK) and 200 μM IBMX for 1 h and were then subjected to seahorse assay with low glucose medium. Data are presented as mean $\pm$ SEM ($n = 5$ biological replicates). *$P < 0.05$; **$P < 0.01$; ns, not significant. (*G*) WT and *AKAP11* KO HEK293T cells were subjected to GS for the indicated times, and cells were then assayed by immunoblotting analysis with the indicated antibodies. (*H*) Quantification of the results from *G* was obtained by normalizing the level of proteins to Actin, respectively, and further to the respective control. Two-way ANOVA was used, and values are presented as mean $\pm$ SEM ($n = 4$). *$P < 0.05$; **$P < 0.01$.
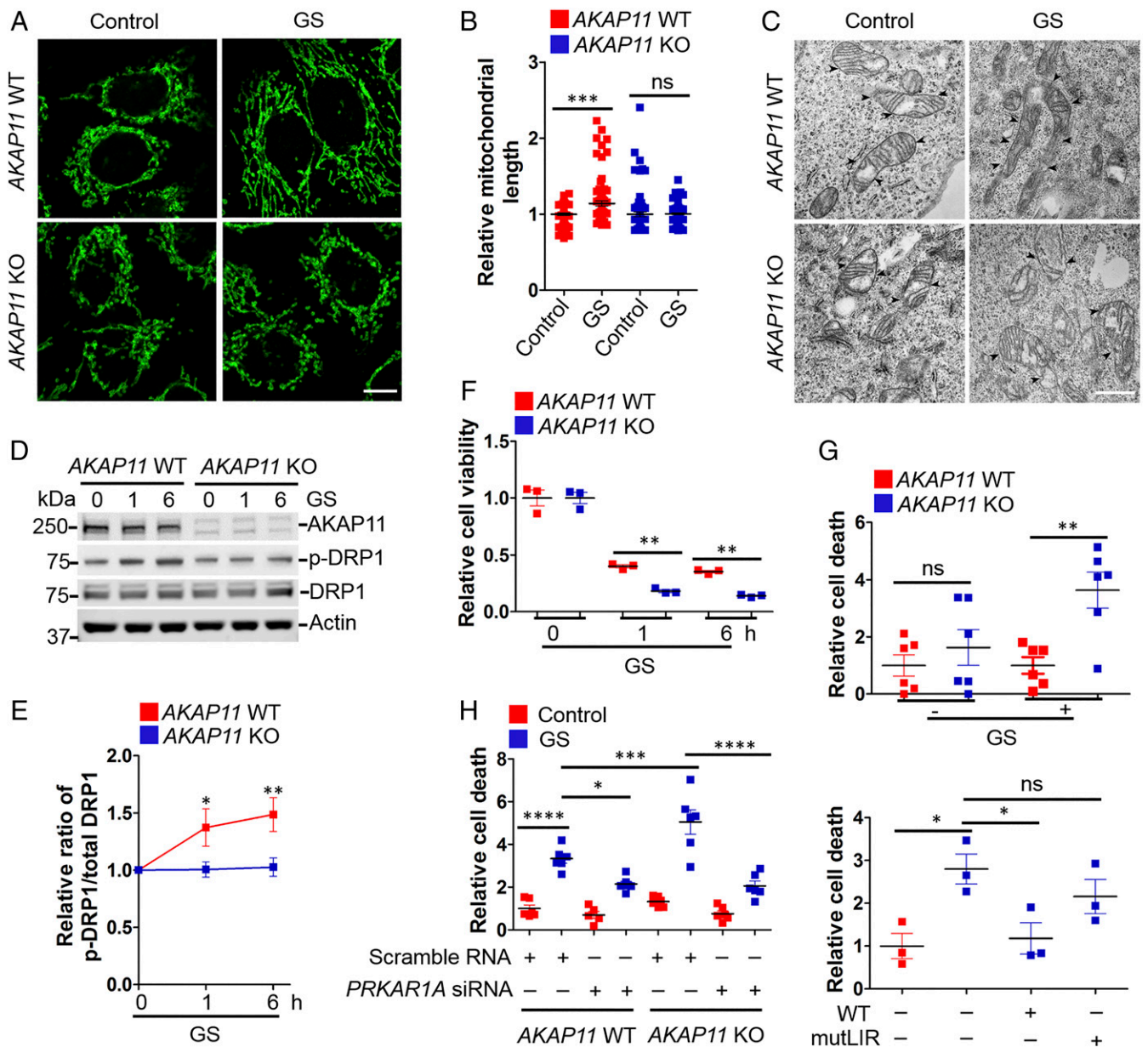
Fig. 6. AKAP11 controls mitochondrial elongation and cell viability through PKA phosphorylation of DRP1 upon glucose starvation (GS). (*A*) WT and *AKAP11* KO HeLa cells were subjected to GS for 1 h and immunostained with TOMM20 antibody. Representative images are shown. (Scale bar, 10 μm.) (*B*) Quantification of the results from *A*. One-way ANOVA was used, and values are presented as mean ± SEM (more than 80 cells were calculated from three independent experiments). ***$P < 0.001$; ns, not significant. (*C*) WT and *AKAP11* KO HeLa cells were subjected to GS for 1 h, and cells were then processed for EM imaging. Representative images are shown. (Scare bar, 1 μm.) (*D*) WT and *AKAP11* KO HeLa cells were subjected to GS for the indicated times and were then assayed by immunoblotting analysis with the indicated antibodies. (*E*) Quantification of the results from *D* was obtained by normalizing the level of proteins to Actin, respectively, and further to the respective control. Two-way ANOVA was used, and values are presented as mean ± SEM ($n = 5$). *$P < 0.05$; **$P < 0.01$. (*F*) WT and *AKAP11* KO HEK293T were subjected to GS for the indicated time and were then measured by cell viability assays. Two-way ANOVA was used, and data are presented as mean ± SEM ($n = 3$). **$P < 0.01$. (*G*) WT and *AKAP11* KO HEK293T were either transfected with HA-AKAP11-WT or HA-AKAP11-mutLIR, then subjected to GS for 24 h, and measured by cell viability assays. One-way ANOVA was used. Data are presented as mean ± SEM. *$P < 0.05$; **$P < 0.01$; ***$P < 0.001$. (*H*) WT and *AKAP11* KO HEK293T were transfected with scramble RNA and *PRKAR1A* siRNA, subjected to GS for 24 h, and measured by cell viability assays. Two-way ANOVA was used. Data are presented as mean ± SEM ***$P < 0.001$; ****$P < 0.0001$.

nutrient for cell replenishment and survival. Here, we identify a critical role of autophagy in boosting the activity of cAMP/PKA, a master regulator of cell metabolism, to maintain cell survival during energy crisis. We show that autophagy selectively degrades PKA inhibitory subunit RIα, which is mediated through AKAP11 receptor. The AKAP11-mediated cAMP/PKA activation results in heightened mitochondrial metabolism in response to glucose starvation and subsequent protection of cell survival

(*SI Appendix*, Fig. S11). We also show that suppression of AKAP11 levels in tumor cells prevents the degradation of RIα and consequently blocks PKA activation, therefore causing inhibition of colony formation of tumor cells. Our results thus throw a light onto autophagy cytoprotection mechanism by demonstrating selective autophagy in RI degradation and PKA activation that fuels the mitochondrial metabolism and confers cell resistance to glucose deprivation in growth. Our results also
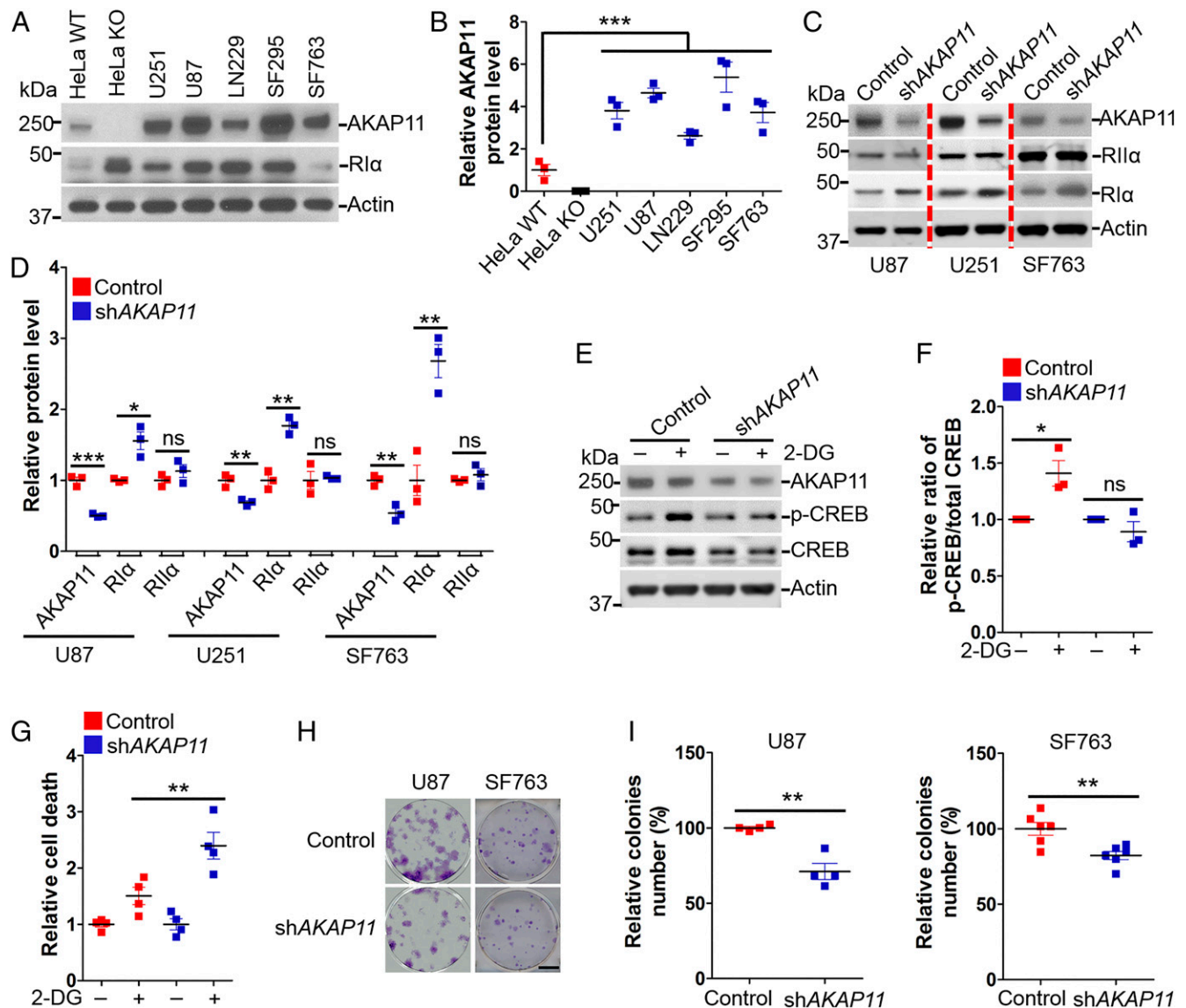
www.manaraa.com

Fig. 7. AKAP11 is required for PKA activation and colony formation of tumor cells. (*A*) Five glioma cell lines (U251, U87, LN229, SF295, and SF763) and HeLa (WT and *AKAP11* KO) cells were assayed by immunoblotting analysis with the indicated antibodies. (*B*) Quantification of the results from *A* was obtained by normalizing the level of AKAP11 to Actin. One-way ANOVA was used, and values are presented as mean ± SEM ($n = 3$). ***$P < 0.001$. (*C*) Control and shRNA-*AKAP11* U87, U251, and SF763 cells were assayed by immunoblotting analysis with the indicated antibodies. (*D*) Quantification of the results from *C* was obtained by normalizing the indicated proteins level to Actin. Unpaired Student's *t* tests were used, and values are presented as mean ± SEM ($n = 3$). *$P < 0.05$; **$P < 0.01$; ***$P < 0.001$; ns, not significant. (*E*) Control and shRNA-*AKAP11* SF763 cells were treated with 20 mM 2-DG for 6 h and were then assayed by immunoblotting analysis with the indicated antibodies. (*F*) Quantification of the results from *E* was obtained by normalizing p-CREB to total CREB levels and further to the respective control. One-way ANOVA was used, and values are presented as mean ± SEM ($n = 3$). *$P < 0.05$; ns, not significant. (*G*) Control and shRNA-*AKAP11* SF763 cells were treated with 20 mM 2-DG for 24 h and were then measured by cell death assays. Two-way ANOVA was used. Data are presented as mean ± SEM ($n = 4$). **$P < 0.01$. (*H*) The colony formation assay was performed in Control and shRNA-*AKAP11* cells (U87 and SF763). The representative images were shown. (Scale bar, 5 mm.) (*I*) The colony formation efficiency in *H* was assessed by normalizing the number of colonies to that in the Control. Unpaired Student's *t* tests were used. Data are presented as mean ± SEM (U87, $n = 4$; SF763, $n = 6$). **$P < 0.01$.

imply that tumor cells may exploit such a metabolic reprogramming system for their growth and resistance to glucose deprivation.

The role for autophagy in sustaining cell metabolism has been well known. The dogma of such a function of autophagy is the supply of metabolic nutrients and fuels as a result of autophagy degradation for cell nourishment and metabolic recycling (6, 40). Our study, however, has advanced the view by unveiling the role for autophagy in directly activating cAMP/PKA signaling that fuels mitochondrial metabolism and confers cell resistance to energy crisis. The tight coupling of autophagic degradation to the

activation of PKA-mediated mitochondria metabolism perhaps provides a means for the cells to rapidly and efficiently recycle digested materials in order to maintain cell survival and growth.

PKA activation is regulated by a variety of intra and extracellular conditions (41, 42). Our study now identifies selective autophagy as a control mechanism for PKA activation by the removal of the inhibitory RI subunit through its interaction with the autophagy receptor AKAP11. Our study reveals that AKAP11 interacts with LC3 via a conserved LIR sequence in AKAP11, which in turn recruits RI to autophagosomes for degradation.

www.manaraa.com

Our study further provides mechanistic insight into how AKAP11-mediated PKA activation regulates cell metabolism. We establish that AKAP11-mediated PKA activation plays a critical role in augmenting mitochondria metabolic function through two lines of evidence: 1) that phosphorylation of CREB drives the increased expression of mitochondrial genes coding for the components of mitochondrial respiratory complexes and 2) that phosphorylation of DRP1 permits mitochondrial elongation or prevents fission of mitochondria. A previous study showed that mitochondria elongate and are spared from degradation during protective autophagy, which is associated with PKA activation and DRP1 phosphorylation. The authors thus concluded that the mitochondrial morphology determines cell fate (39). While the observation is consistent with our finding with regard to glucose starvation–induced mitochondria elongation, it could result from the AKAP11-mediated PKA activation, which causes DRP1 phosphorylation and mitochondrial elongation upon nutrient starvation to offer cell protection.

Multiple lines of evidence have demonstrated the activation of cAMP/PKA in tumor growth (43). An omics-based analysis of cancer tissues revealed a central role for the heightened cAMP/PKA activity as well as autophagy in the resistance of tumor cells to the glucose starvation (31). This study suggests the significance for the interplay between autophagy, cAMP/PKA, and cellular metabolism in tumor growth and resistance to glucose starvation. However, the exact mechanism underlying their relationship in tumor growth remains unclear. We posit that, based on our observations, tumor cells may exploit AKAP11-mediated PKA activation to fuel mitochondrial metabolism for the benefit of tumor growth under nutrient-poor conditions. Indeed, highly active autophagy has been reported across many different types of tumors, and the phenomenon was dubbed "autophagy addiction," as tumor cells rely on autophagy for survival (44–46). On the other hand, increasing evidence has demonstrated that activation of PKA drives tumorigenesis. In fact, activation of PKA signaling caused by rare human genetic variants are associated with the development of a spectrum of neuroendocrine tumors (47, 48). Using a large scale and unbiased kinase profiling, a very recent study reported that the PKA signaling pathway is active and central for the development of small cell lung cancer, a common and fatal form of neuroendocrine cancer (49). The emerging evidence has convincingly shown the contribution of PKA activation to the growth of certain types of tumors through reprogramming cell metabolism. Our study has now suggested a causal relationship between selective autophagy degradation and PKA activation, therefore connecting the two important pathways in regulation of cell metabolism and tumor growth. We predict that many other metabolic stress conditions or pathological conditions in cells beyond tumors might also activate AKAP11-mediated PKA activation for cell survival and growth.

Our findings also raise many questions. For instance, the exact mechanism whereby glucose starvation induces selective degradation of RIα through AKAP11 autophagy receptor is unclear. In addition to glucose starvation, whether other biological or pathological conditions could activate AKAP11-mediated PKA activation process, and the potential consequence(s) of such PKA activation in those conditions remain(s) to be studied. In addition, AKAP11-mediated PKA activation rejuvenates mitochondrial metabolism, which contrasts mitophagy that degrades mitochondria through autophagy lysosome. Therefore, how mitophagy, which removes mitochondria, is regulated distinctively from the increase of mitochondrial metabolism caused by AKAP11-mediated selective autophagy warrants future investigation. Finally, our finding opens an avenue for investigation of the interplay of PKA signaling, metabolic regulation, mitochondria and autophagy in various physiological as well as metabolic disease conditions. It further implies a therapeutic target for the treatment of metabolic diseases including cancer.

Materials and Methods

Cell Culture. HeLa cells, HEK293T cells, HCT116 cells, MEFs, and stably expressing GFP-LC3B HEK293T cells were maintained in Dulbecco's modified Eagle's medium (Invitrogen) supplemented with 50 μg/mL penicillin and streptomycin (Invitrogen) and 10% FBS ([fetal bovine serum] Invitrogen). HEK293T $Atg7^{(-/-)}$ and the corresponding control were a generous gift from Dr. Harper J. Wade (Harvard Medical School). U87 MG, LN229, U251 MG, SF295, and SF763 were obtained from the American Type Culture Collection and University of California San Francisco Neurosurgery Tissue Bank, respectively, and maintained in Roswell Park Memorial Institute medium (Gibco, 11875-093) supplemented with 50 μg/mL penicillin and streptomycin and 10% FBS. Transient transfection was performed using Lipofectamine 2000 or 3000 (Invitrogen) as per the manufacturer's instruction.

Plasmids and Reagents. Human HA–AKAP11-WT construct was provided by Dr. Kikuchi Akira (Osaka University). HA-AKAP11-mutLIR was constructed using a Quick-Change Lightning Site-Directed Mutagenesis Kit. GST-LC3A, -LC3B, and -GABARAP were ordered from Addgene. For FLAG-RIα construct, human RIα was subcloned from pDONR22-RIα (Addgene) into the 3X Flag-CMV-7.1 vectors (Addgene). pCMV-3X Flag-LC3 (Addgene), AKAR4 (Addgene), MG132 (Calbiochem, 474791), Puromycin (Thermo Fisher Scientific, A11138-03), Polybrene (Sigma-Aldrich, H9268), Lipofectamine 2000/3000 (Thermo Fisher Scientific, 11668-019/L3000-015), ethylenediaminetetraacetic acid (EDTA)-free phosphatase inhibitor mixture and protease inhibitor mixture (Thermo Fisher Scientific, 1861281), IPTG (isopropyl-β-ᴅ-thiogalactopyranoside, Sigma-Aldrich, 367-93-1), PEI (Polyethylenimine, Sigma-Aldrich, 408717), Forskolin (Sigma-Aldrich, F3917), IBMX (Sigma-Aldrich, I5879), EBSS (Sigma-Aldrich, E2888), Dynabeads protein G (Thermo Fisher Scientific, 10004D), QuikChange Lightning Site-Directed Mutagenesis Kits (Agilent Technologies, 210518), polyvinylidene difluoride membrane (Millipore, IPFL00010), Scramble siRNA (Thermo Fisher Scientific, 4390846), PRKAR1A siRNA (Thermo Fisher Scientific, S287), and Bicinchoninic Acid (BCA) Protein Assay Reagent Kit (Thermo Fisher Scientific, 23228) were also utilized.

Antibodies. The following antibodies were used: AKAP11 (Life Span Bio Sciences, LS-C374339-200), RIα (Cell Signaling Technology, #5675; BD Bio Sciences, 610165), RIIα (BD Bio Sciences, 612242), p62 (Progen Biotechnik, GP62-C), LC3A/B (Cell Signaling Technology, #12741), Ubiquitin (Dako, Z0458), β-Actin (Cell Signaling Technology, 3700), GFP (Thermo Fisher Scientific, A11122), FLAG-M2 (Sigma-Aldrich, F1804), HA (Santa Cruz Biotechnology, sc-7392), CREB (EMD Millipore, MAB5432), p-CREB Ser133 (EMD Millipore, 06-519), NDUFS4 (Santa Cruz Biotechnology, sc-100567), MTCOII (Proteintech, Cosmo Bio, 55070-1-AP), p-DRP1 Ser637 (Sigma-Aldrich, SAB4301399), DRP1 (Abcam, ab56788), and TOMM20 (Santa Cruz Biotechnology, sc-17764).

Immunoblotting and Immunoprecipitation. Total cellular lysates were prepared in a cell lysate buffer (1% Nonidet P-40, 50 mM Tris HCl pH 7.4, 150 mM NaCl, 1 mM EDTA, 0.25% sodium deoxycholate, complete protease and phosphatase inhibitor). After centrifugation at 13,000 g at 4 °C for 30 min, supernatants were collected and subjected to BCA assay and were then resolved by sodium dodecyl sulphate–polyacrylamide gel electrophoresis. For immunoprecipitation (IP), cellular lysates were prepared in IP buffer (100 mM NaCl, 10 mM Tris HCl pH 7.4, 1% Nonidet P-40, 2 mM EDTA, complete protease and phosphatase inhibitor mixture). After centrifugation at 13,000 g at 4 °C for 30 min. Supernatants were collected and subjected to BCA assay, followed by incubation with the indicated antibodies overnight at 4 °C. Lysates were further incubated with Dynabeads protein G at 4 °C for 1.5 h and washed with phosphate-buffered solution (PBS) (0.1% Triton X-100) five times and subjected to immunoblotting assay. Detection was performed by either LI-COR Odyssey or medical film processor. Immunoblotting results were analyzed by using either Image Studio or ImageJ.

Fluorescence Microscopy. For colocalization of AKAP-11 and RIα with endogenous LC3, HeLa cells with indicated genotypes were treated with EBSS plus 100 nM BafA1 for 2 h. After treatment, cells were fixed with paraformaldehyde/methanol fixation protocol: briefly, cells were fixed in 4% paraformaldehyde at room temperature (RT) for 15 min and washed with PBS three times for 5 min. Cells were then permeabilized with ice-cold methanol at −20 °C for 15 min and were subsequently washed with PBS three times for 5 min. After washing, cells were subjected to immunostaining assay as described previously (50). Briefly, cells blocked with blocking buffer (5% goat serum and 0.3%

Triton X-100 in PBS) at RT for 1 h. Cells were then incubated with primary and secondary antibodies accordingly in incubating buffer (3% bovine serum albumin and 0.3% Triton X-100 in PBS) at 4 °C overnight. Cells were then mounted with mounting medium (ProLong Gold anti-fade mountant, Invitrogen) and examined under Carl Zeiss confocal microscopes (LSM780 system). Images were taken with 100× oil immersion objective lense at RT, and image acquisition was performed using Zen2012 software. Digitized images were analyzed and processed by using ImageJ software as described previously (50). Briefly, quantification of puncta was determined by scoring green positive structures ≥0.1 μm/cell, and colocalization ratios were obtained by using tManders2 values. For mitochondrial analysis, mitochondrial length was measured by using the "MINA" plugin from Stuart laboratory for ImageJ, according to literature (51). For the FRET biosensor assay, WT and *AKAP11* KO HEK293T cells were glucose starved as per indicated time, followed by live imaging in a dark room at cell growth condition. Images were acquired on a Leica inverted DMi8 Live Cell Imaging Microscope (Leica Microsystems). FRET signals were acquired by using one excitation filter and two emission filters. Exposure time was 200 ms, and images were acquired at 40× magnification every 30 s for 5 min per sample.

Purification of Proteins and In Vitro Pull-Down Assay. GST-LC3A, -LC3B, and -GABARAP were expressed in *Escherichia coli* BL21 (DE3) cells, which were induced by IPTG. Cellular lysates were prepared in TNE buffer (10 mM Tris HCl pH 8.0, 150 mM NaCl, 1 mM EDTA, and 1% Nonidet P-40) on ice for 30 min. After centrifugation at 13,000 g at 4 °C for 20 min, supernatants were incubated with Glutathione Sepharose 4B (GE Healthcare, 17-0756-01) at 4 °C overnight. Pellets were then washed three times with TNE buffer and were incubated with cellular lysates from HEK293T cells expressing either HA-AKAP11 or HA-AKAP11-mutLIR at 4 °C overnight. After washing four times with TNE buffer, pellets were mixed with loading buffer and subjected to immunoblotting assay.

Preparation of Brain Lysates of *Atg7F/F-SynCre* and *Atg14F/F-SynCre*. All animal studies were performed in compliance with the Institutional Animal Care and Use Committee at Icahn School of Medicine at Mount Sinai. To generate *Atg7F/F-SynCre* and *Atg14F/F-SynCre* mice, floxed Atg7 (*Atg7F/F*) and Atg14 (*Atg14F/F*) mice were crossed with *Atg7F/+-SynCre* and *Atg14F/+-SynCre* mice. Whole brains were collected from the indicated mice with 1 to 2 mo old and homogenized with buffer containing 50 mM Tris HCl, pH 7.5, 150 mM NaCl, and 1% Triton X-100. Brain lysates were subjected to immunoblotting assay.

Preparation of Lentivirus and Establishment of *AKAP11* KO Cells. The guide RNA (gRNA) guiders for *AKAP11* KO were synthesized (Integrated DNA Technologies) and cloned into lentiCRISPR version 2 plasmid (Addgene). Lentiviruses were packaged using three plasmids (Addgene), PMDL, RSV, VSVG. Briefly, 90% confluent HEK293T cells in 10 cm dishes were cotransfected with 20 μg respective plasmids (2:1:0.5:0.5) using PEI. At 6 h posttransfection, the medium was replaced with fresh medium and collected at 30 h posttransfection. The medium containing viruses was filtered through a 0.45 μm pore syringe filter. For transduction, 90% confluent HEK293T and HeLa cells were infected with the medium containing gRNA lentiviral particles and 10 μg/mL polybrene. At 48 h posttransfection, the medium was replaced with selection medium containing 2 μg/mL puromycin, and new selection medium was subsequently switched every 3 d. After 7 d, puromycin-resistant cells were harvested and seeded into a 96-well plate as single cell per well by serial dilution. Individual clones were harvested and expanded. PCR products from each clone were sequenced and protein expression was confirmed by immunoblotting assay.

Quantitative Real-Time PCR. For qRT-PCR, total RNA was extracted from WT, *Atg7* KO, and *AKAP11* KO HEK293T cells, which were subjected to glucose starvation for the indicated times by using the eukaryote RNA extraction kit (Qiagen, 74104). Then, 0.5 μg of total RNA (in a final volume of 20 μL) was used to synthesize complementary DNA (cDNA) using Affinity Script Reverse transcriptase (Agilent technology). The primers used to measure the differential expression of genes are listed in the supplementary material (*SI Appendix*, Table S1). The housekeeping gene *β-Actin* was used as a reference. qRT-PCR was performed on cDNA from each sample by using the SYBR Green Master Mix ABI 7900HT Fast Real-Time PCR System. Amplification was conducted for 1 cycle at 95 °C for 2 min, followed by 40 cycles at 95 °C for 15 s, annealing at 55 °C for 15 s,

and extension at 72 °C for 30 s. The mRNA quantity of each gene was analyzed by using standardized qPCR facility method for copy number determination.

Electron Microscopy (EM). HeLa WT and *AKAP11* KO cells were treated as indicated. Cells were grown on chambered permanox slides (Electron Microscopy Sciences [EMS]) and were immersion fixed with 2% paraformaldehyde and 2% glutaraldehyde in 0.01 M sodium cacodylate solution (EMS) at 4 °C overnight. Sections were rinsed in 0.1 M sodium cacodylate buffer, followed by a quick rinse with ddH$_2$O. Cells were postfixed with 1% osmium tetroxide/ddH$_2$0, dehydrated, and followed by embedding in a modified BEEM embedding capsule (EMS) according to a standard procedure. Ultra-thin sections were collected on copper 300 mesh grids (EMS) using a Coat-Quick adhesive pen (EMS), counter stained with 1% uranyl acetate and lead citrate, and were then imaged on a Hitachi 7000 electron microscope (Hitachi High-Technologies) using an advantage charge-coupled device camera (Advanced Microscopy Techniques). Images were adjusted for brightness and contrast using ImageJ software.

Mitochondrial Respiration Assay. WT and *AKAP11* KO HEK293T and HeLa cells were seeded in a XF24 cell culture microplate (Agilent Technologies, product No. 100777-004) at a density of around 20,000 cells/well. After an overnight incubation in an incubator with 5% CO$_2$ at 37 °C, cells were washed with PBS and subjected to glucose starvation or low glucose incubation with seahorse medium (Agilent Technologies, product No. 102353-100) supplemented with 1 mM pyruvate, 2 mM glutamine, and 10 mM glucose for 1 h. OCR (oxygen consumption rate) was measured using the Seahorse XF24 Analyzer (Agilent Technologies) under basal level and in response to Oligomycin (1.5 μM), FCCP (Carbonyl cyanide 4-(trifluoromethoxy) phenylhydrazone) (1.0 μM), and Antimycin/Rotenone (0.5 μM) according to the manufacturer's instructions (Agilent Seahorse XF Cell Mito Stress Test Kit, product No. 103015-100).

Establishment of the Stably Transduced Control and shRNA-*AKAP11* Cells. To generate the stable Control and sh*AKAP11* knockdown cells, 90% confluent glioblastoma cells U87, U251, and SF763 were infected with lentiviral particles carrying control mixed shRNA against *AKAP11* (sh*AKAP11*) (Santa Cruz Biotechnology, control, sc-108080; *AKAP11*, sc-105049-V) and 10 μg/mL polybrene. At 48 h posttransfection, the medium was replaced with selection medium containing 2 μg/mL puromycin and new selection medium was subsequently switched every 3 d. After 7 d, puromycin-resistant cells were harvested and subjected to immunoblotting assay to confirm the indicated gene's expression.

Colony Formation, Cell Death, and Cell Viability Assay. Cells were seeded into 6-well plates at 1,000 cells per well in 2 mL of medium. The medium was switched with a fresh one every 7 d during the experimental period. After 2 to 3 wk, colonies were washed with PBS and fixed in 100% methanol for 30 min, stained with 0.5% crystal violet, and counted. Cells were treated as indicated and were then subjected to cell death (BioVision, K311-400) and cell viability (Abcam, ab155902) assays according to the manufacturer's instructions.

Statistical Analysis. Statistical analyses were performed using GraphPad Prism version 5.0. Student's *t* test and one-way (followed by Tukey's post-hoc test) or two-way (followed by Bonferroni's post-hoc test) ANOVA were used. $P \le 0.05$ was considered statistically significant.

Data Availability. All study data are included in the article and/or *SI Appendix*.

1. N. Mizushima, Autophagy: Process and function. *Genes Dev.* **21**, 2861–2873 (2007).
2. B. Levine, G. Kroemer, Biological functions of autophagy genes: A disease perspective. *Cell* **176**, 11–42 (2019).
3. Z. Yue, S. Jin, C. Yang, A. J. Levine, N. Heintz, Beclin 1, an autophagy gene essential for early embryonic development, is a haploinsufficient tumor suppressor. *Proc. Natl. Acad. Sci. U.S.A.* **100**, 15077–15082 (2003).
4. X. Qu *et al.*, Promotion of tumorigenesis by heterozygous disruption of the beclin 1 autophagy gene. *J. Clin. Invest.* **112**, 1809–1820 (2003).
5. A. C. Kimmelman, E. White, Autophagy and tumor metabolism. *Cell Metab.* **25**, 1037–1043 (2017).
6. L. Galluzzi, F. Pietrocola, B. Levine, G. Kroemer, Metabolic control of autophagy. *Cell* **159**, 1263–1276 (2014).

Deng et al.
Selective autophagy of AKAP11 activates cAMP/PKA to fuel mitochondrial metabolism and tumor cell growth

PNAS | 11 of 12
https://doi.org/10.1073/pnas.2020215118

CELL BIOLOGY

www.manaraa.com

7. H. Chino, T. Hatta, T. Natsume, N. Mizushima, Intrinsically disordered protein TEX264 mediates ER-phagy. *Mol. Cell* **74**, 909–921.e6 (2019).

8. K. Mochida *et al.*, Receptor-mediated selective autophagy degrades the endoplasmic reticulum and the nucleus. *Nature* **522**, 359–362 (2015).

9. Y. C. Kim, K. L. Guan, mTOR: A pharmacologic target for autophagy regulation. *J. Clin. Invest.* **125**, 25–32 (2015).

10. M. M. Mihaylova, R. J. Shaw, The AMPK signalling pathway coordinates cell growth, autophagy and metabolism. *Nat. Cell Biol.* **13**, 1016–1023 (2011).

11. O. Torres-Quesada, J. E. Mayrhofer, E. Stefan, The many faces of compartmentalized PKA signalosomes. *Cell. Signal.* **37**, 1–11 (2017).

12. H. Yang, L. Yang, Targeting cAMP/PKA pathway for glycemic control and type 2 diabetes therapy. *J. Mol. Endocrinol.* **57**, R93–R108 (2016).

13. S. Monterisi, M. Zaccolo, Components of the mitochondrial cAMP signalosome. *Biochem. Soc. Trans.* **45**, 269–274 (2017).

14. S. J. Cherra, 3rd *et al.*, Regulation of the autophagy protein LC3 by phosphorylation. *J. Cell Biol.* **190**, 533–539 (2010).

15. X. Zhao *et al.*, Endothelial PKA activity regulates angiogenesis by limiting autophagy through phosphorylation of ATG16L1. *eLife* **8**, e46380 (2019).

16. F. Torres-Quiroz, M. Filteau, C. R. Landry, Feedback regulation between autophagy and PKA. *Autophagy* **11**, 1181–1183 (2015).

17. R. K. Dagda *et al.*, Mitochondrially localized PKA reverses mitochondrial pathology and dysfunction in a cellular model of Parkinson's disease. *Cell Death Differ.* **18**, 1914–1923 (2011).

18. P. Mishra, D. C. Chan, Metabolic regulation of mitochondrial dynamics. *J. Cell Biol.* **212**, 379–387 (2016).

19. C. Kim, C. Y. Cheng, S. A. Saldanha, S. S. Taylor, PKA-I holoenzyme structure reveals a mechanism for cAMP-dependent activation. *Cell* **130**, 1032–1043 (2007).

20. W. Wong, J. D. Scott, AKAP signalling complexes: Focal points in space and time. *Nat. Rev. Mol. Cell Biol.* **5**, 959–970 (2004).

21. S. H. Koo *et al.*, The CREB coactivator TORC2 is a key regulator of fasting glucose metabolism. *Nature* **437**, 1109–1111 (2005).

22. K. Lemaire, S. Van de Velde, P. Van Dijck, J. M. Thevelein, Glucose and sucrose act as agonist and mannose as antagonist ligands of the G protein-coupled receptor Gpr1 in the yeast *Saccharomyces cerevisiae*. *Mol. Cell* **16**, 293–299 (2004).

23. A. U. Syed *et al.*, Adenylyl cyclase 5-generated cAMP controls cerebral vascular reactivity during diabetic hyperglycemia. *J. Clin. Invest.* **129**, 3140–3152 (2019).

24. L. B. Lester, V. M. Coghlan, B. Nauert, J. D. Scott, Cloning and characterization of a novel A-kinase anchoring protein. AKAP 220, association with testicular peroxisomes. *J. Biol. Chem.* **271**, 9460–9465 (1996).

25. M. E. Day *et al.*, Isoform-specific targeting of PKA to multivesicular bodies. *J. Cell Biol.* **193**, 347–363 (2011).

26. Y. Kabeya *et al.*, LC3, a mammalian homologue of yeast Apg8p, is localized in autophagosome membranes after processing. *EMBO J.* **19**, 5720–5728 (2000).

27. A. B. Birgisdottir, T. Lamark, T. Johansen, The LIR motif–Crucial for selective autophagy. *J. Cell Sci.* **126**, 3237–3247 (2013).

28. G. A. Gonzalez, M. R. Montminy, Cyclic AMP stimulates somatostatin gene transcription by phosphorylation of CREB at serine 133. *Cell* **59**, 675–680 (1989).

29. C. Depry, M. D. Allen, J. Zhang, Visualization of PKA activity in plasma membrane microdomains. *Mol. Biosyst.* **7**, 52–58 (2011).

30. F. Chiaradonna, Y. Pirola, F. Ricciardiello, R. Palorini, Transcriptional profiling of immortalized and K-ras-transformed mouse fibroblasts upon PKA stimulation by forskolin in low glucose availability. *Genom. Data* **9**, 100–104 (2016).

31. R. Palorini *et al.*, Protein kinase A activation promotes cancer cell resistance to glucose starvation and anoikis. *PLoS Genet.* **12**, e1005931 (2016).

32. J. Li *et al.*, Mitochondrial elongation-mediated glucose metabolism reprogramming is essential for tumour cell survival during energy stress. *Oncogene* **36**, 4901–4912 (2017).

33. K. Birsoy *et al.*, Metabolic determinants of cancer cell sensitivity to glucose limitation and biguanides. *Nature* **508**, 108–112 (2014).

34. R. Acin-Perez, D. L. Gatti, Y. Bai, G. Manfredi, Protein phosphorylation and prevention of cytochrome oxidase inhibition by ATP: Coupled mechanisms of energy metabolism regulation. *Cell Metab.* **13**, 712–719 (2011).

35. D. De Rasmo *et al.*, Phosphorylation pattern of the NDUFS4 subunit of complex I of the mammalian respiratory chain. *Mitochondrion* **10**, 464–471 (2010).

36. D. De Rasmo *et al.*, Intramitochondrial adenylyl cyclase controls the turnover of nuclear-encoded subunits and activity of mammalian complex I of the respiratory chain. *Biochim. Biophys. Acta* **1853**, 183–191 (2015).

37. S. Papa *et al.*, cAMP-dependent protein kinase regulates post-translational processing and expression of complex I subunits in mammalian cells. *Biochim. Biophys. Acta* **1797**, 649–658 (2010).

38. A. D. Rouillard *et al.*, The harmonizome: A collection of processed datasets gathered to serve and mine knowledge about genes and proteins. *Database (Oxford)* **2016**, baw100 (2016).

39. L. C. Gomes, G. Di Benedetto, L. Scorrano, During autophagy mitochondria elongate, are spared from degradation and sustain cell viability. *Nat. Cell Biol.* **13**, 589–598 (2011).

40. J. D. Rabinowitz, E. White, Autophagy and metabolism. *Science* **330**, 1344–1348 (2010).

41. A. P. Kornev, S. S. Taylor, Dynamics-driven allostery in protein kinases. *Trends Biochem. Sci.* **40**, 628–647 (2015).

42. L. K. Langeberg, J. D. Scott, Signalling scaffolds and local organization of cellular behaviour. *Nat. Rev. Mol. Cell Biol.* **16**, 232–244 (2015).

43. S. Naviglio *et al.*, Protein kinase A as a biological target in cancer therapy. *Expert Opin. Ther. Targets* **13**, 83–92 (2009).

44. M. T. Rosenfeldt, K. M. Ryan, The role of autophagy in tumour development and cancer therapy. *Expert Rev. Mol. Med.* **11**, e36 (2009).

45. J. D. Mancias, A. C. Kimmelman, Targeting autophagy addiction in cancer. *Oncotarget* **2**, 1302–1306 (2011).

46. J. Y. Guo *et al.*, Activated Ras requires autophagy to maintain oxidative metabolism and tumorigenesis. *Genes Dev.* **25**, 460–470 (2011).

47. F. Beuschlein *et al.*, Constitutive activation of PKA catalytic subunit in adrenal Cushing's syndrome. *N. Engl. J. Med.* **370**, 1019–1028 (2014).

48. Y. Cao *et al.*, Activating hotspot L205R mutation in PRKACA and adrenal Cushing's syndrome. *Science* **344**, 913–917 (2014).

49. G. L. Coles *et al.*, Unbiased proteomic profiling uncovers a targetable GNAS/PKA/PP2A axis in small cell lung cancer stem cells. *Cancer Cell* **38**, 129–143.e7 (2020).

50. Z. Deng *et al.*, ALS-FTLD-linked mutations of SQSTM1/p62 disrupt selective autophagy and NFE2L2/NRF2 anti-oxidative stress pathway. *Autophagy* **16**, 917–931 (2020).

51. A. J. Valente, L. A. Maddalena, E. L. Robb, F. Moradi, J. A. Stuart, A simple imageJ macro tool for analyzing mitochondrial network morphology in mammalian cell culture. *Acta Histochem.* **119**, 315–326 (2017).